Transparent, Flexible Conducting Hybrid Multilayer Thin Films of Multiwalled Carbon Nanotubes with Graphene Nanosheets

Tae-Keun Hong, Dong Wook Lee, Hyun Jung Choi, Hyeon Suk Shin,* and Byeong-Su Kim*

Interdisciplinary School of Green Energy and School of NanoBio and Chemical Engineering, Ulsan National Institute of Science and Technology (UNIST), Ulsan 689-798, Korea

ABSTRACT We developed a simple, versatile method of integrating hybrid thin films of reduced graphene oxide (RGO) nanosheets with multiwalled carbon nanotubes (MWNTs) *via* LbL assembly. This approach involves the electrostatic interactions of two oppositely charged suspensions of the RGO nanosheet with MWNTs. This method affords a hybrid multilayer of graphenes with excellent control over the optical and electrical properties. Moreover, the hybrid multilayer exhibits a significant increase of electronic conductivity after the thermal treatment, producing transparent and conducting thin films possessing a sheet resistance of 8 kΩ/sq with a transmittance of 81%. By taking advantage of the conducting network structure of MWNTs, which provides an additional flexibility and mechanical stability of RGO nanosheets, we demonstrate the potential application of hybrid graphene multilayer as a highly flexible and transparent electrode. Because of the highly versatile and tunable properties of LbL-assembled thin films, we anticipate that the general concept presented here offers a unique potential platform for integrating active carbon nanomaterials for advanced electronic, energy, and sensor applications.

KEYWORDS: graphene oxide nanosheets · carbon nanotubes · layer-by-layer assembly · transparent conducting electrode · flexible film

With their unique and novel properties, carbon nanomaterials, including carbon nanotubes, carbon fibers, and graphenes, have generated a great deal of interest in academia and industry. Among them, graphene, a single layer of two-dimensional carbon lattice, has recently emerged as a promising novel nanomaterial with its remarkable electrical, chemical, and mechanical properties.[1,2] While earlier fundamental studies have been initiated from the micromechanical cleavage of highly crystalline graphite for generation of high-quality graphene sheets,[2] recent efforts are geared toward producing the graphene sheets in a controlled, scalable, and reproducible manner. For example, suspensions of stable graphene oxide (GO) can be readily obtained by ultrasonication of chemically oxidized graphite oxide, offering the potential of creating large-scale graphene thin films.[3] A number of approaches have been made to assemble these well-dispersed oxidized or chemically reduced graphene oxide nanosheets into thin films with tailorable properties and architectures, including vacuum filtration,[4−8] Langmuir−Blodgett assembly,[9,10] and direct chemical vapor deposition.[11−13] Although this recent progress presents facile routes for fabrication of thin films composed of exclusively graphenes, it continues to be a challenging endeavor to realize a nanoscale uniform blend of hybrid structure of graphene nanosheets with other nanomaterials in a well-defined composition and structure. In that regard, Yang and co-workers have recently demonstrated the successful hybridization of chemically converted graphenes with carbon nanotubes in a solution process for a potential polymer solar cell application.[14]

Alternatively, one simple and versatile method to assemble hybrid graphene structure is using layer-by-layer (LbL) assembly, as it can create highly tunable, conformal thin films and functional surfaces with nanometer-scale control over the film composition and structure.[15,16] LbL assembly can also allow the incorporation of diverse nanostructures, including carbon nanotubes, nanoparticles, polymers, and biomolecules in a single platform, each with a distinct structure and composition by the choice of materials and controlling the sequence of layering.[17−20] The integration of graphenes into multilayer thin films has been recently demonstrated with LbL techniques but are limited to the hybrid structures with polymers.[21−23]

*Address correspondence to shin@unist.ac.kr, bskim19@unist.ac.kr.

Received for review March 15, 2010 and accepted June 28, 2010.

Published online July 6, 2010. 10.1021/nn100897g

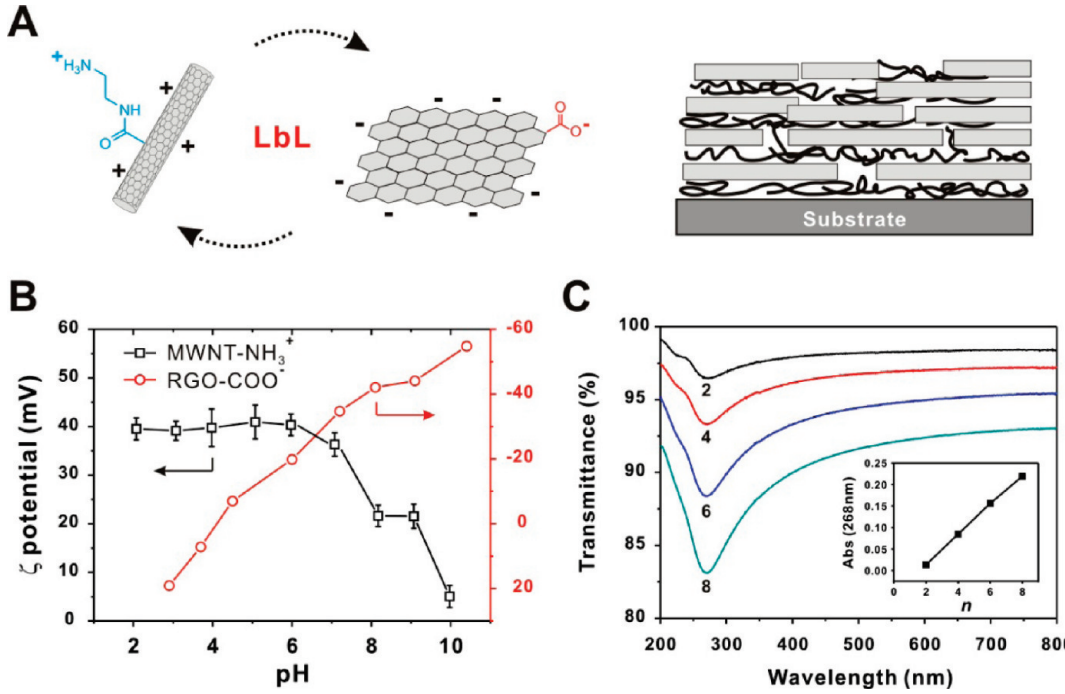

Figure 1. (A) Schematic representation of hybrid LbL multilayer of MWNTs and RGO; (B) pH-dependent ζ-potential of chemically functionalized MWNT−NH_3^+ and RGO−COO^- suspensions; (C) UV/vis growth profile of $(MWNT/RGO)_n$ multilayer. (Inset) Absorbance at 268 nm with the number of bilayers (*n*). Note that the dimension of MWNTs and RGO is not to scale.

In this article, we present a simple, novel strategy for creating multilayered thin films of highly conducting reduced graphene oxide (RGO) nanosheets with multiwalled carbon nanotubes (MWNTs) *via* LbL assembly. Specifically, we have constructed hybrid multilayers employing the electrostatic interactions between positively charged MWNTs and negatively charged exfoliated nanosheets of RGO (Figure 1). The integration of MWNTs not only provides the electronic conductivity but also affords mechanical flexibility of the hybrid film, allowing the electronic contact of graphene nanosheets by bridging the gaps between graphene sheets. We demonstrated furthermore that the assembled hybrid multilayer can be utilized as a flexible, transparent conducting electrode possessing high electrical conductivity and transparency while allowing significant flexibility. Although there have been approaches to coupling the unique properties of carbon nanotubes and/or graphenes with the versatility of LbL assembly for electronic applications,[23−26] this system is unique in that the multilayer thin films consist of carbon nanomaterials exclusively. This is important because we can take advantage of the unique properties of carbon nanomaterials without incorporation of other organic materials that can potentially sacrifice the intrinsic electrochemical or electronic properties of carbon nanomaterials; we can also integrate active carbon nanomaterials with other nanomaterials at a nanoscale precision for fine-tuning the electrical and optical properties of the transparent electrodes for future optoelectronics.[27,28]

According to the modified Hummers method,[29] we have prepared graphene oxide suspensions from commercially available graphite powder, followed by sonication for exfoliation of graphite oxide to graphene oxide (GO) suspension. The chemical functional groups introduced on the surface of the graphene oxide sheet, such as carboxylic acids (COOH), render the prepared GO negatively charged (GO−COO^-). Chemical reduction of GO suspension was carried out by adding hydrazine in the presence of ammonia to prevent the aggregation of the resulting RGO suspension.[6] As determined by ζ-potential measurement, the prepared RGO suspension exhibited a fairly good colloidal stability (−55 mV at pH 10) (Figure 1B) and remained clearly dispersed for more than a month without noticeable aggregation. The RGO sheets show a broad lateral size distribution of 0.5−2 μm with a clear view of graphene edges by atomic force microscopy (AFM) (see Supporting Information). In parallel, positively charged MWNTs were initially prepared from the oxidation of MWNTs in the presence of strong acids to afford MWNTs functionalized with carboxylic acids (MWNT−COOH). Subsequently, introduction of amine groups (NH_2) onto the surface of MWNT−COOH was achieved through the reaction between carboxylic acids and excess ethylenediamine mediated with *N*-ethyl-*N*′-(3-dimethylaminopropyl)carbodiimide methiodide (EDC). This leads to a positively charged MWNT suspension (MWNT−NH_3^+) that is stable over a wide span of pH conditions (Figure 1B). X-ray photoelectron spectroscopy (XPS) further supports the pres-

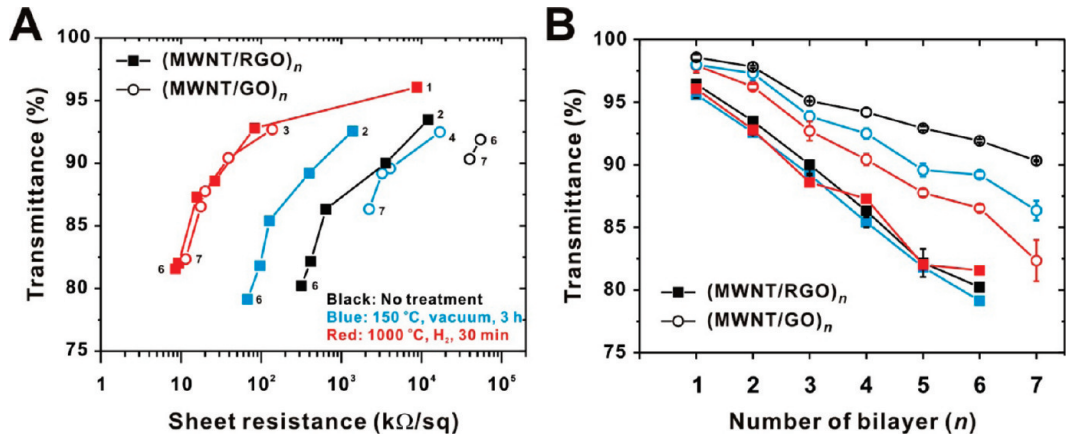

Figure 2. (A) Function of sheet resistance *vs* transmittance changes of hybrid films after thermal treatment. Number on the symbol represents the number of bilayers (*n*). (B) Transmittance of hybrid films as a function of number of bilayers (*n*) under different thermal treatment. Solid squares represent $(MWNT/RGO)_n$ films, and open circles represent $(MWNT/GO)_n$ films. Black line corresponds to as-assembled film, blue is for films treated with mild temperature (150 °C in vacuum for 3 h), and red corresponds to films with high-temperature treatment (1000 °C in H_2 for 30 min). Transmittance was measured at 550 nm, and a sheet resistance was measured with a four-point probe.

ence of the reactive functional groups on the surface of the MWNT, such as amide (402 eV) and amine groups (400 eV) (see Supporting Information).

On the basis of the electrostatic interactions, multilayer thin films were assembled by repeatedly spin-coating the suspensions of $MWNT-NH_3^+$ and $RGO-COO^-$ on a planar silicon wafer or quartz slide to afford the multilayer in the architecture of $(MWNT/RGO)_n$ (n = number of bilayers).[30] We monitored the linear growth of multilayers by the gradual increase of characteristic UV/vis absorbance of RGO within the film (λ_{max} = 268 nm) (Figure 1C), which also indicates the successful reduction of GO.[6] Moreover, the transmittance of the hybrid film at 550 nm was easily adjustable by assembly parameters such as concentration, pH, and spin-assembly conditions (see Supporting Information). In particular, upon decreasing the pH of MWNT suspensions from 6.5 to 3.5 at fixed pH of RGO (pH 10), we found that the thickness of a 5 bilayer film measured by ellipsometry decreases from 14 to 11 nm. This is due to charge increase of amine groups in $MWNT-NH_3^+$ by lowering pH, leading to less adsorption on the negatively charged $RGO-COO^-$ layer to balance the surface charges. This pH-tailorable behavior of LbL thin films is similarly observed with weak polyelectrolytes such as poly(acrylic acid) and poly(allylamine hydrochloride), where pH can alter the degree of ionization of weak polyelectrolytes, eventually leading to differences in film thickness and morphology of the resulting LbL films.[31] It is also suggested that the interpenetration of carbon nanotubes may play an important role in influencing the adsorption with respect to the charge density along the carbon nanotubes.[19]

We demonstrated furthermore that the assembled hybrid multilayer can be utilized as a transparent conducting electrode possessing high electrical conductivity with varying transparency. In comparison to the electrically conducting RGO, we also considered using unreduced GO to prepare the hybrid film of $(MWNT/GO)_n$ and evaluated the effect of chemical and thermal reduction methods in terms of increasing the conductivity of the resulting hybrid multilayer without sacrificing the transmittance of the films. The hybrid multilayer of $(MWNT/GO)_n$ was similarly assembled by the LbL approach using $GO-COO^-$ suspensions instead of $RGO-COO^-$.

As reported previously, high-temperature graphitization is known to be the most effective in deoxygenating the graphene film and restoring its conductivity.[32] We have therefore investigated the effect of thermal treatment in order to increase and restore the conductivity of the hybrid multilayer, a prerequisite for a large-scale transparent conducting electrode (Figure 2). The conductivity of both $(MWNT/RGO)_n$ and $(MWNT/GO)_n$ hybrid films was determined by measuring a sheet resistance (R_s) of the film with a four-point probe. As expected, the $(MWNT/RGO)_n$ multilayer exhibited a measurable conductivity after the film deposition becomes uniform over the areas (>2 bilayer), while $(MWNT/GO)_n$ film did not display a measurable conductivity (too high to measure R_s) until there were 6 bilayers, possibly due to the large number of structural defects present in GO and the low degree of percolation network created by MWNTs. The sheet resistance values gradually decreased with the number of bilayers owing to the increased connectivity of graphene sheets and carbon nanotube networks, as shown in the scanning electron microscopy (SEM) images (see Figure 3). Upon mild thermal treatment at 150 °C, the sheet resistance of the as-assembled $(MWNT/RGO)_n$ multilayer shows an order of magnitude decrease, while that of the $(MWNT/GO)_n$ multilayer decreases only modestly

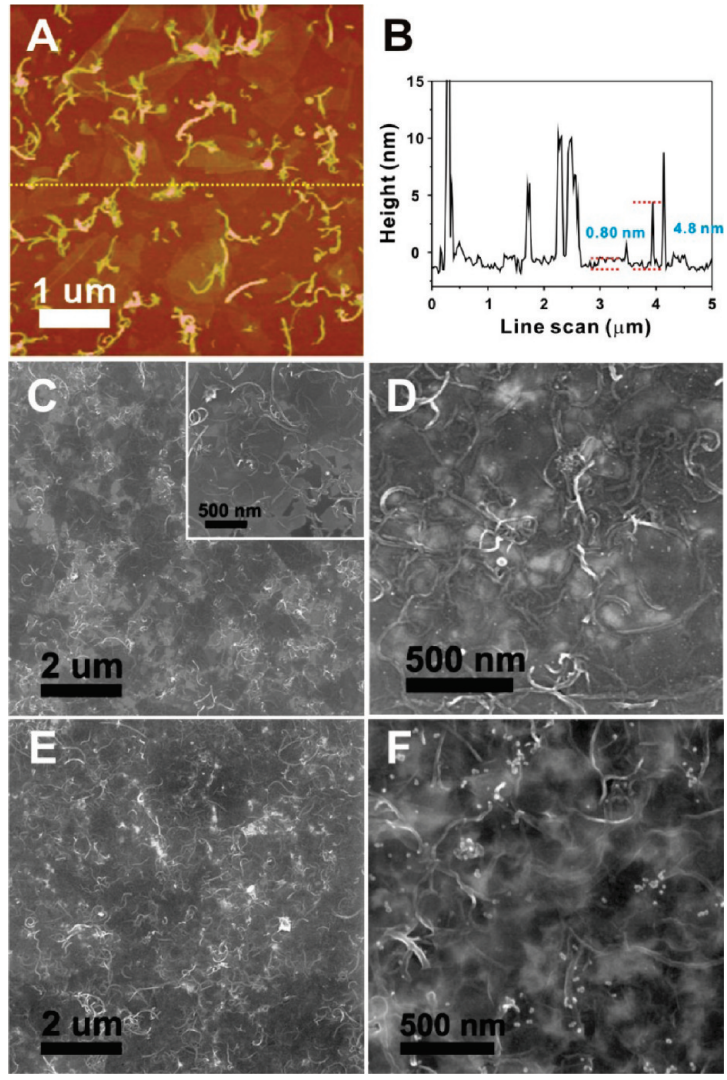

Figure 3. Representative surface morphology of a hybrid multilayer of $(MWNT/RGO)_n$ and $(MWNT/RGO)_n$. (A,B) AFM image of as-assembled $(MWNT/RGO)_1$ multilayer with corresponding surface profile. (C) SEM image of as-assembled $(MWNT/RGO)_5$ multilayer; (inset) high-resolution image. (D) $(MWNT/RGO)_5$ multilayer after thermal reduction at 1000 °C under H_2. (E) SEM image of as-assembled $(MWNT/GO)_5$ multilayer and (F) $(MWNT/GO)_5$ multilayer after chemical treatment with hydrazine.

(Figure 2A). The modest thermal treatment is particularly useful when applying this hybrid film to be fully compatible with a flexible substrate such as poly(ethylene terephthlate) (PET). However, in order to create multilayers of RGO with the highest electrical conductivity, we have further treated the hybrid multilayers under reductive environments at high temperature (1000 °C, H_2, 30 min). This results in a significant decrease of sheet resistance for both multilayers; for example, a $(MWNT/RGO)_6$ film with a thickness of 11 nm exhibits a sheet resistance of 8 kΩ/sq with a transparency of 81% (Figure 2A). In comparison to previously reported values of a few layers of chemically reduced GO films with a sheet resistance of *ca.* 4 MΩ/sq[33] and 10^2-10^3 Ω/sq after annealing at 1100 °C,[32] this hybrid multilayer of MWNTs and RGO gives a similar level of conductivity. XPS study further indicates that the highly enhanced electrical conductivity after the heat treatment is due to the restoration of sp^2 nature of graphene (Figure 4). In parallel to the increase of conductivity, we found that the high-temperature treatment generally decreases the transmittance of the $(MWNT/RGO)_n$ film by 1.3%, while that of the $(MWNT/GO)_n$ film diminished considerably (8%) upon post-thermal treatment (Figure 2B).

With the restoration of sp^2 nature of graphene, the transmittance tends to decrease in general; however, this effect is more pronounced in the case of the unreduced $(MWNT/GO)_n$ multilayer. Taken together, the $(MWNT/RGO)_n$ multilayer exhibits a high conductivity with a predictable transmittance upon thermal treatment. The significantly enhanced conductivity of $(MWNT/RGO)_n$ hybrid films compared to $(MWNT/GO)_n$ arises from a more complete reduction

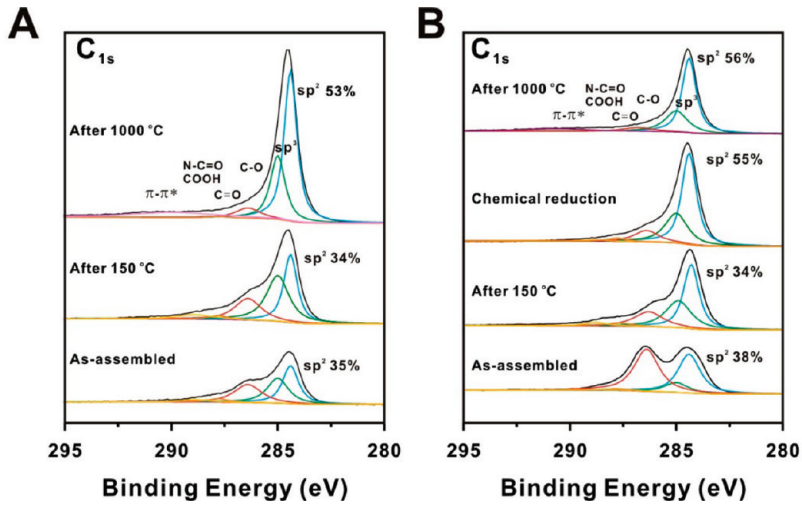

Figure 4. High-resolution C1s XPS spectra of hybrid multilayer of (A) $(MWNT/RGO)_5$ and (B) $(MWNT/GO)_5$ multilayers under different post-treatments. The fraction of sp^2 carbon is indicated in each figure.

of GO in the solution phase before the deposition, and this finding suggests that, through further process optimization, RGO hybrid films could become an attractive candidate for a large-scale transparent conducting film.

The surface morphology of the hybrid multilayer was observed by AFM and SEM (Figure 3). As illustrated in Figure 3A, the one bilayer film consists of a few overlapping sheets of RGO with MWNTs scattered on the surface. As the deposition progresses, the entire film displays graphene nanosheets that are overlayering with a randomly distributed percolating network of MWNTs (Figure 3C,D). This is similarly observed in the control $(MWNT/GO)_5$ film as well (Figure 3E). We observed that the film morphology did not change significantly after the thermal reduction process except the edges of the graphene nanosheets became less distinct after high-temperature treatment, suggesting that the graphene sheets have merged together with the restoration of the structures. In contrast, the $(MWNT/GO)_5$ film undergoes a dramatic change in morphology of the graphene sheet after chemical reduction by hydrazine, as similarly observed in a previous report (Figure 3F).[32]

XPS studies were employed to monitor the progress of characteristic binding energy of C1s peaks corresponding to the hybrid multilayers under different chemical and thermal treatment (Figure 4). The deconvoluted C1s spectra provided detailed surface functional groups present on the MWNT and RGO, including sp^2-hybridized graphitic carbons (284.5 eV), sp^3-hybridized saturated carbons (285.0 eV), C−O (286.4 eV), C═O (287.8 eV), amide (288.1 eV), and carboxyl groups (288.9 eV), which are all in good agreement with previous works.[34] In general, the relative intensities of each peak vary upon post-treatment (either by chemical or thermal) with a clear demonstration of the restoration of the graphitic sp^2 carbon peak. Furthermore, upon chemical reduction of the $(MWNT/GO)_5$ multilayer, the carboxyl groups decrease, consistent with observations made previously, and suggest that reduction of GO has taken place successfully.[23] After the hydrazine reduction or mild thermal treatment, the multilayer still contains a small amount of nitrogen species, attributable to either the presence of covalently attached nitrogen functional groups on MWNTs as well as surface-attached hydrazine onto graphene sheets by chemical reactions, such as epoxide ring opening.[35] On the other hand, we could not observe any signature of a nitrogen peak after the high-temperature treatment, indicating that all nitrogen-containing functional groups (amines and amides) have evolved from the surfaces of MWNTs, possibly in the form of N_2 gas. Interestingly, the oxygen-containing groups are not completely removed even after the high-temperature treatment, as also observed by Chhowalla and co-workers.[34] It is also of note that the broad $\pi-\pi^*$ satellite peak (290.6 eV) is visible in both hybrid multilayers.[34]

Consistent with the XPS data, the Raman spectra displayed characteristic features of chemically functionalized MWNTs and GO, including D (1346 cm^{-1}, disorder due to sp^3 carbon bonds), G (1596 cm^{-1}, C−C stretching in graphitic lattice), and 2D modes (2698 cm^{-1}) (see Supporting Information). The relative area ratio of the D to G peaks obtained (I_D/I_G) was used to provide information of structural defects present in the hybrid multilayer.[36] As-prepared hybrid multilayers of $(MWNT/RGO)_5$ show I_D/I_G of 1.66 ± 0.12, and that for $(MWNT/GO)_5$ was 1.82 ± 0.03. With the progress of post-thermal treatment, these values decreased modestly to 1.59 ± 0.03 for $(MWNT/RGO)_5$ and 1.68 ± 0.14 for $(MWNT/GO)_5$ because of the increased cluster size of sp^2 carbon, consistent with previous studies.[34] In addition, the 2D band becomes more pronounced with high-temperature treatment, further proving the prominent recovery of

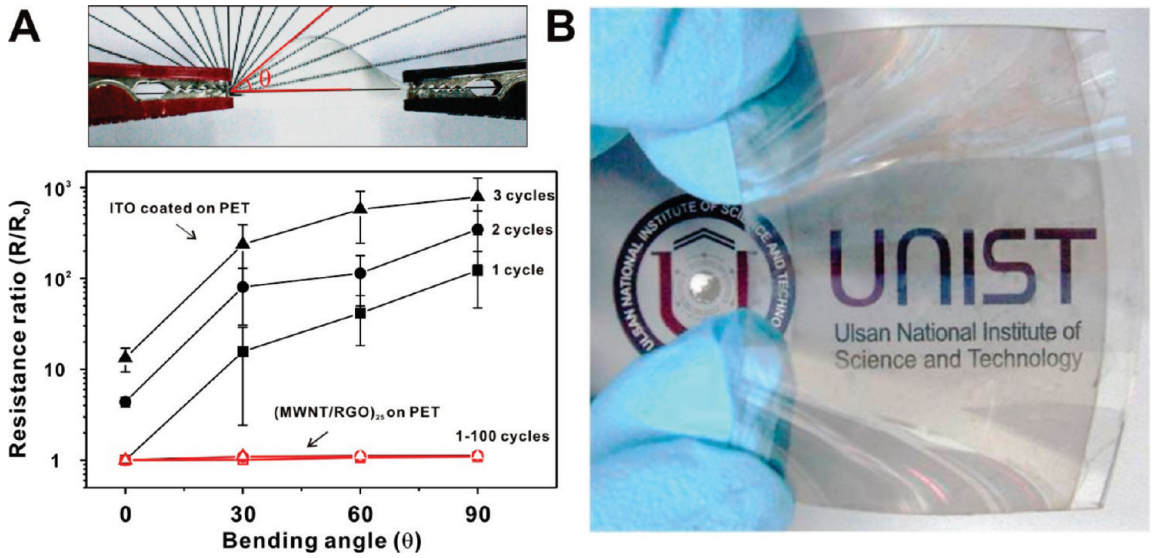

Figure 5. Bending experiment of hybrid multilayer film deposited on a flexible PET. (A) Changes of surface resistance of $(MWNT/RGO)_{25}$ coated on PET and ITO-coated PET under different bending angles with an experimental setup. (B) Image of $(MWNT/RGO)_{25}$ hybrid thin film on a PET substrate after mild thermal treatment.

the sp^2-hybridized network within the graphene sheets, in accord with the decrease in transmittance presented above.

A unique feature of these LbL-assembled hybrid films of $(MWNT/RGO)_n$ can be further demonstrated by use of a flexible substrate such as PET. We compared the resistance changes of our hybrid $(MWNT/RGO)_{25}$ multilayer coated on PET with a commercial ITO-coated PET under forced bending experiments (Figure 5). Although our $(MWNT/RGO)_{25}$ multilayer coated on the PET substrate exhibits a relatively higher sheet resistance of 57 kΩ/sq after mild thermal treatment (150 °C, vacuum for 3 h), its electrical conducting properties are maintained under excessively bending conditions (90° bending angle corresponds to approximate tensile strain of 6.3%) and retained the initial values over multiple cycles (100 cycles). This is in marked contrast with ITO-coated PET, which undergoes irreversible loss of electrical conductivity with the increased level of cracks in the rigid inorganic nanostructure of ITO upon bending the substrate. The superior flexibility of hybrid $(MWNT/RGO)_n$ films stems from the presence of the network structure of MWNTs, which provides additional flexibility and mechanical stability of RGO nanosheets by conductively bridging the nanosheets. We believe this finding will provide the basis for development of hybrid graphene films for future large-area transparent and flexible electrode applications.

CONCLUSION

In summary, we have developed a novel method of integrating hybrid thin films of RGO nanosheets with MWNT *via* LbL assembly. This approach employs the electrostatic interactions of two oppositely charged suspensions of RGO nanosheets with MWNTs. This method affords a hybrid multilayer of $(MWNT/RGO)_n$ with excellent control over the optical and electrical properties. Moreover, the hybrid multilayer exhibits a significant increase of electronic conductivity after the thermal treatment, producing transparent and conducting thin films possessing a sheet resistance of 8 kΩ/sq with a transparency of 81% at 550 nm. Furthermore, we demonstrated the application of the assembled hybrid graphene thin film as a flexible electrode, which will enable the assembly of a graphene-based electrode in a scalable, large-area transparent and flexible electrode. Because of the highly versatile and tunable properties of LbL-assembled thin films, we anticipate that the general concept presented here offers a unique potential platform for integrating active carbon nanomaterials for advanced electronic, energy, and sensor applications.

METHODS

Preparation of Negatively Charged RGO and Positively Charged MWNTs. Graphite oxide was synthesized from graphite (BayCarbon) by a modified Hummers method and exfoliated to give a brown dispersion of graphene oxide (GO) under ultrasonication. The resulting GO suspension (10.0 mL, 0.50 mg/mL) was mixed with 10.0 μL of hydrazine solution (35 wt % in water, Aldrich) and 70.0 μL of ammonia solution (30%, Samchun). After stirring for 10 min, the reaction mixture was heated to 95 °C for 1 h to afford the reduced graphene oxide (RGO) nanosheets used in this study. Positively charged MWNTs were synthesized according to the published protocol with a modification.[19] Carboxylic acid functionalized MWNTs (Hanwha, CM 100) were prepared with strong acid treatment using H_2SO_4/HNO_3 at 70 °C for 2 h. The suspensions of carboxylated MWNTs (80 mL, 0.50 mg/mL) were reacted with excess ethylenediamine (8.0 mL) under stirring for 5 h in the presence of 800 mg of *N*-ethyl-*N*′-(3-dimethylaminopropyl)carbodiimide methiodide (EDC, 98%, Alfa Aesar). The resulting suspension was dialyzed (MWCO

12000−14000) for a few days to remove any byproduct and residuals during functionalization. The resulting suspensions of RGO−COO^- and MWNT−NH_3^+ were briefly sonicated prior to LbL assembly.

Layer-by-Layer Assembly. Silicon or quartz substrate was cleaned by piranha solution to remove any organic contamination and treated with oxygen plasma to introduce a hydrophilic surface. Positively charged MWNT−NH_3^+ solution (0.50 mg/mL) at pH 6.5 was dropped on the substrate, which was loaded on a spin-coater (ACE-200, Dong Ah Tech), maintained for 30 s as a waiting period, and spun at 2000 rpm for 30 s. As a rinsing step, pH-adjusted water was dropped on the substrate and followed the same protocol used for MWNT−NH_3^+ deposition. Next, negatively charged RGO (or GO) solution (0.50 mg/mL) was spin-coated with the same procedures, followed by the rinsing step with pH-adjusted water, which affords one bilayer of MWNT and RGO sheets with a notation of $(MWNT/RGO)_1$. These procedures were repeated to achieve the desired number of bilayers and also for $(MWNT/GO)_n$ multilayers.

Characterizations. Zeta-potential of colloidal suspensions was measured using a ζ-potential analyzer (Malvern, Zetasizer nanozs). The transmittance of the hybrid films was characterized by using the UV/vis spectroscopy (VARIAN, Cary 5000). The thickness of the hybrid film on a silicon substrate was measured using an ellipsometry (EC-400 and M-2000 V, J.A. Woollam Co. Inc.). Surface morphology of the samples was investigated using atomic force microscopy (AFM, Nanoscope V, Veeco) *via* a tapping mode and scanning electron microscopy (SEM, FEI, NOVA NANOSEM 230). Functionalized MWNTs, RGO, and assembled multilayers were characterized by XPS (Thermo Fisher, K-alpha). Raman spectra were obtained, and the D/G area ratio was fitted after baseline correction (Witec, alpha-300M). The sheet resistance of the hybrid films was measured by using a four-point probe method (Advanced Instrument Technology, CMT-SR1000N).

Acknowledgment. This research was supported by WCU (World Class University) program through the Korea Science and Engineering Foundation funded by the Ministry of Education, Science and Technology (R31-2008-000-20012-0).

Supporting Information Available: Additional characterization data of AFM, XPS, and Raman spectra. This material is available free of charge *via* the Internet at http://pubs.acs.org.

REFERENCES AND NOTES

1. Novoselov, K. S.; Geim, A. K.; Morozov, S. V.; Jiang, D.; Zhang, Y.; Dubonos, S. V.; Grigorieva, I. V.; Firsov, A. A. Electric Field Effect in Atomically Thin Carbon Films. *Science* **2004**, *306*, 666–669.
2. Novoselov, K. S.; Jiang, D.; Schedin, F.; Booth, T. J.; Khotkevich, V. V.; Morozov, S. V.; Geim, A. K. Two-Dimensional Atomic Crystals. *Proc. Natl. Acad. Sci. U.S.A.* **2005**, *102*, 10451–10453.
3. Eda, G.; Fanchini, G.; Chhowalla, M. Large-Area Ultrathin Films of Reduced Graphene Oxide as a Transparent and Flexible Electronic Material. *Nat. Nanotechnol.* **2008**, *3*, 270–274.
4. Dikin, D. A.; Stankovich, S.; Zimney, E. J.; Piner, R. D.; Dommett, G. H. B.; Evmenenko, G.; Nguyen, S. T.; Ruoff, R. S. Preparation and Characterization of Graphene Oxide Paper. *Nature* **2007**, *448*, 457–460.
5. Xu, Y. X.; Bai, H.; Lu, G. W.; Li, C.; Shi, G. Q. Flexible Graphene Films *via* the Filtration of Water-Soluble Noncovalent Functionalized Graphene Sheets. *J. Am. Chem. Soc.* **2008**, *130*, 5856–5857.
6. Li, D.; Muller, M. B.; Gilje, S.; Kaner, R. B.; Wallace, G. G. Processable Aqueous Dispersions of Graphene Nanosheets. *Nat. Nanotechnol.* **2008**, *3*, 101–105.
7. Hernandez, Y.; Nicolosi, V.; Lotya, M.; Blighe, F. M.; Sun, Z. Y.; De, S.; McGovern, I. T.; Holland, B.; Byrne, M.; Gun'ko, Y. K.; *et al.* High-Yield Production of Graphene by Liquid-Phase Exfoliation of Graphite. *Nat. Nanotechnol.* **2008**, *3*, 563–568.
8. Park, S.; An, J. H.; Jung, I. W.; Piner, R. D.; An, S. J.; Li, X. S.; Velamakanni, A.; Ruoff, R. S. Colloidal Suspensions of Highly Reduced Graphene Oxide in a Wide Variety of Organic Solvents. *Nano Lett.* **2009**, *9*, 1593–1597.
9. Li, X. L.; Zhang, G. Y.; Bai, X. D.; Sun, X. M.; Wang, X. R.; Wang, E.; Dai, H. J. Highly Conducting Graphene Sheets and Langmuir−Blodgett Films. *Nat. Nanotechnol.* **2008**, *3*, 538–542.
10. Cote, L. J.; Kim, F.; Huang, J. X. Langmuir−Blodgett Assembly of Graphite Oxide Single Layers. *J. Am. Chem. Soc.* **2009**, *131*, 1043–1049.
11. Kim, K. S.; Zhao, Y.; Jang, H.; Lee, S. Y.; Kim, J. M.; Kim, K. S.; Ahn, J. H.; Kim, P.; Choi, J. Y.; Hong, B. H. Large-Scale Pattern Growth of Graphene Films for Stretchable Transparent Electrodes. *Nature* **2009**, *457*, 706–710.
12. Li, X. S.; Cai, W. W.; Colombo, L.; Ruoff, R. S. Evolution of Graphene Growth on Ni and Cu by Carbon Isotope Labeling. *Nano Lett.* **2009**, *9*, 4268–4272.
13. Li, X. S.; Zhu, Y. W.; Cai, W. W.; Borysiak, M.; Han, B. Y.; Chen, D.; Piner, R. D.; Colombo, L.; Ruoff, R. S. Transfer of Large-Area Graphene Films for High-Performance Transparent Conductive Electrodes. *Nano Lett.* **2009**, *9*, 4359–4363.
14. Tung, V. C.; Chen, L. M.; Allen, M. J.; Wassei, J. K.; Nelson, K.; Kaner, R. B.; Yang, Y. Low-Temperature Solution Processing of Graphene−Carbon Nanotube Hybrid Materials for High-Performance Transparent Conductors. *Nano Lett.* **2009**, *9*, 1949–1955.
15. Decher, G. Fuzzy Nanoassemblies: Toward Layered Polymeric Multicomposites. *Science* **1997**, *277*, 1232–1237.
16. Hammond, P. T. Form and Function in Multilayer Assembly: New Applications at the Nanoscale. *Adv. Mater.* **2004**, *16*, 1271–1293.
17. Mamedov, A. A.; Kotov, N. A.; Prato, M.; Guldi, D. M.; Wicksted, J. P.; Hirsch, A. Molecular Design of Strong Single-Wall Carbon Nanotube/Polyelectrolyte Multilayer Composites. *Nat. Mater.* **2002**, *1*, 190–194.
18. Kim, B.-S.; Park, S. W.; Hammond, P. T. Hydrogen-Bonding Layer-by-Layer Assembled Biodegradable Polymeric Micelles as Drug Delivery Vehicles from Surfaces. *ACS Nano* **2008**, *2*, 386–392.
19. Lee, S. W.; Kim, B.-S.; Chen, S.; Shao-Horn, Y.; Hammond, P. T. Layer-by-Layer Assembly of All Carbon Nanotube Ultrathin Films for Electrochemical Applications. *J. Am. Chem. Soc.* **2009**, *131*, 671–679.
20. Wang, Y.; Angelatos, A. S.; Caruso, F. Template Synthesis of Nanostructured Materials *via* Layer-by-Layer Assembly. *Chem. Mater.* **2008**, *20*, 848–858.
21. Shen, J. F.; Hu, Y. Z.; Li, C.; Qin, C.; Shi, M.; Ye, M. X. Layer-by-Layer Self-Assembly of Graphene Nanoplatelets. *Langmuir* **2009**, *25*, 6122–6128.
22. Kong, B. S.; Geng, J. X.; Jung, H. T. Layer-by-Layer Assembly of Graphene and Gold Nanoparticles by Vacuum Filtration and Spontaneous Reduction of Gold Ions. *Chem. Commun.* **2009**, 2174–2176.
23. Kim, Y. K.; Min, D. H. Durable Large-Area Thin Films of Graphene/Carbon Nanotube Double Layers as a Transparent Electrode. *Langmuir* **2009**, *25*, 11302–11306.
24. Shim, B. S.; Tang, Z. Y.; Morabito, M. P.; Agarwal, A.; Hong, H. P.; Kotov, N. A. Integration of Conductivity Transparency, and Mechanical Strength into Highly Homogeneous Layer-by-Layer Composites of Single-Walled Carbon Nanotubes for Optoelectronics. *Chem. Mater.* **2007**, *19*, 5467–5474.
25. Shim, B. S.; Zhu, J.; Jan, E.; Critchley, K.; Kotov, N. A. Transparent Conductors from Layer-by-Layer Assembled SWNT Films: Importance of Mechanical Properties and a New Figure of Merit. *ACS Nano* **2010**, DOI: 10.1021/nn100026n.
26. Park, H. J.; Kim, J.; Chang, J. Y.; Theato, P. Preparation of Transparent Conductive Multilayered Films Using Active Pentafluorophenyl Ester Modified Multiwalled Carbon Nanotubes. *Langmuir* **2008**, *24*, 10467–10473.
27. Kumar, A.; Zhou, C. W. The Race To Replace Tin-Doped Indium Oxide: Which Material Will Win? *ACS Nano* **2010**, *4*, 11–14.

28. De, S.; Coleman, J. N. Are There Fundamental Limitations on the Sheet Resistance and Transmittance of Thin Graphene Films? *ACS Nano* **2010**, *4*, 2713–2720.
29. Hummers, W. S.; Offeman, R. E. Preparation of Graphitic Oxide. *J. Am. Chem. Soc.* **1958**, *80*, 1339.
30. The bilayer is to represent the Lbl film consists of two components sush as MWNT and RGO in this case, and should not represent the graphene bilayer, meaning double-stack of graphene sheets.
31. Shiratori, S. S.; Rubner, M. F. pH-Dependent Thickness Behavior of Sequentially Adsorbed Layers of Weak Polyelectrolytes. *Macromolecules* **2000**, *33*, 4213–4219.
32. Becerril, H. A.; Mao, J.; Liu, Z.; Stoltenberg, R. M.; Bao, Z.; Chen, Y. Evaluation of Solution-Processed Reduced Graphene Oxide Films as Transparent Conductors. *ACS Nano* **2008**, *2*, 463–470.
33. Gilje, S.; Han, S.; Wang, M.; Wang, K. L.; Kaner, R. B. A Chemical Route to Graphene for Device Applications. *Nano Lett.* **2007**, *7*, 3394–3398.
34. Mattevi, C.; Eda, G.; Agnoli, S.; Miller, S.; Mkhoyan, K. A.; Celik, O.; Mostrogiovanni, D.; Granozzi, G.; Garfunkel, E.; Chhowalla, M. Evolution of Electrical, Chemical, and Structural Properties of Transparent and Conducting Chemically Derived Graphene Thin Films. *Adv. Funct. Mater.* **2009**, *19*, 2577–2583.
35. Compton, O. C.; Dikin, D. A.; Putz, K. W.; Brinson, C.; Nguyen, S. T. Electrically Conductive Alkylated Graphene Paper *via* Chemical Reduction of Amine-Functionalized Graphene Oxide Paper. *Adv. Mater.* **2010**, *22*, 892–896.
36. Stankovich, S.; Dikin, D. A.; Piner, R. D.; Kohlhaas, K. A.; Kleinhammes, A.; Jia, Y.; Wu, Y.; Nguyen, S. T.; Ruoff, R. S. Synthesis of Graphene-Based Nanosheets *via* Chemical Reduction of Exfoliated Graphite Oxide. *Carbon* **2007**, *45*, 1558–1565.